PROCEEDINGS OF MOSES2023 CONFERENCE
4TH INTERNATIONAL CONFERENCE ON MODELLING AND OPTIMISATION OF SHIP ENERGY SYSTEMS
26-27 OCTOBER 2023, DELFT, NETHERLANDS

Decentralized Power Sharing with Frequency Decoupling for a Fuel Cell-Battery DC Shipboard Power System

Timon Kopka[*a], Foivos Mylonopoulos[a], Andrea Coraddu[a,b], and Henk Polinder[a]

[a]Department of Maritime and Transport Technology, Delft University of Technology, The Netherlands
[b]Netherlands Defence Academy, The Netherlands
[*]Corresponding author: t.kopka@tudelft.nl

Abstract

The maritime industry is under increasing pressure to reduce its carbon footprint by adopting new energy generation and storage technologies in shipboard power systems (SPS). Fuel cells (FCs) show great potential as primary power sources when hybridized with energy storage systems (ESS). Integrating different technologies in future SPS requires the coordination of power generation and storage modules, which can be facilitated by DC technology with power electronics interfaces. However, studies on FC integration have primarily focused on small-scale applications with centralized control architectures. There has been little research on the modular control of multiple FC and battery modules in SPS. This study proposes a decentralized droop-based power sharing approach with load frequency decoupling to efficiently utilize power system modules based on their dynamic capabilities. The proposed strategy further incorporates decentralized voltage regulation and state-of-charge (SoC) management functions. The methodology was applied to a short-sea cargo vessel with an FC-battery DC power system. The results indicate that the mission load profile can be satisfied while limiting fluctuations in the FC output power. Moreover, the proposed strategy achieves the same voltage regulation performance as a centralized proportional-integral (PI) controller and can be easily tuned to achieve load frequency decoupling with the desired time constant. Finally, a comparative analysis shows how the trade-off between the dynamic operation of the FC and the discharge depth of the ESS is affected by the choice of time constant.

Keywords: DC power distribution, Frequency decoupling, Fuel cells, Power sharing, Shipboard power system

1 INTRODUCTION

Whereas the maritime industry could rely on internal combustion engines and a direct-driven topology in the past, technological advances as well as regulatory and environmental challenges drive innovation in the design of shipboard power systems (SPSs) [1]. The electrification and incorporation of energy storage systems (ESSs) into an integrated power system (IPS) are among the key trends observed in power system designs [2]. Moreover, the aim of reducing the dependency on fossil fuels has brought fuel cells (FCs) into play as an alternative to diesel generators as power supplies [3], [4]. One central enabling technology facilitating the integration of FC-battery hybrid systems is the DC distribution technology. This is further supported by power electronics interfaces that achieve a high degree of controllability of power flows in the system [5]. Recent developments further point to the benefits of integrating these subsystems in a modular fashion, making them easily replaceable and allowing for an expansion of the SPS [6], [7].

A challenge lies in the question of how multiple power generation and storage modules with different dynamic and steady-state characteristics can be efficiently coordinated [8]. A power system is required to provide sufficient power under fluctuating loads while minimizing fuel costs and component wear [9]. FCs, in particular, suffer from high efficiency losses and lifetime degradation if not operated with low output gradient and within an efficient operation band [10]. Considering the presence of different power generation characteristics and the goal of achieving an easily reconfigurable power system with plug-and-play (PnP) capability, a suitable control strategy is required to meet these requirements. A decentralized control architecture is generally regarded as advantageous in terms of scalability and reconfigurability of the power system [11], [12]. Droop control using a virtual resistance is the most common method for achieving decentralized power sharing. However, this leads to voltage deviations and inefficient power sharing under transient loads [9], [13]. A goal in hybrid power systems is to decouple the load frequencies using the battery to cover high load gradients so that the main supply can operate efficiently and at low stress [2].

DOI: https://doi.org/10.59490/moses.2023.670

The approaches for coordinated control in the FC-battery SPS found in the literature are dominated by centralized solutions, typically involving only a single FC and battery. This is realized, e.g., using PI-controllers as in [14]–[16] or via rule-based approaches as in [16]–[19]. Load-frequency separation is also a popular objective for the control of a hybrid energy storage system (HESS) [20]–[22]. The current literature fails to account for larger hydrogen-based DC SPS with multiple parallel components, in which one centralized controller is no longer feasible. Moreover, such centralized solutions do not offer the desired modular characteristics. Accordingly, this study aims to develop a method for dynamic power sharing among multiple FC and ESS in an SPS using a decentralized architecture as a scalable and reconfigurable solution.

A virtual impedance-based approach for decentralized HESS-control using capacitive droop elements was described in [23]. This concept is extended by an inductive droop controller in this study to achieve droop-based frequency decoupling for batteries and FCs. The decentralized architecture facilitates the extension of the power system with further components, which can be parameterized according to their dynamic characteristics to cover the total load demand. Additionally, each local controller's reference voltage is constantly adapted to achieve a secondary function. Whereas the reference of the FC droop control is adapted such that the DC bus voltage is regulated to its nominal value, the voltage adaption in the ESS aims to manage and balance their state of charge (SoC). Accordingly, the main contribution of this study is a decentralized coordinated control strategy for DC SPS, that achieves a simultaneous load frequency decoupling, voltage regulation, and SoC management. The developed methodology is finally showcased in numerical simulations at the example of a short-sea cargo ship.

The remainder of this paper is organized as follows. Section 2 elaborates on the SPS design considered in this study. The modeling is described in Section 3. The main contribution of this study, i.e., the coordinated control strategy, is detailed in Section 4. Finally, Section 5 presents the simulation scenarios and results, followed by an overview of the main conclusions of this study in Section 6.

2 SYSTEM DESCRIPTION

The proposed control strategy was developed for all-electric ships (AESs) with predominantly propulsive loads, which is the case for cargo vessels. Hence, the main power demand is for the electric propulsion. On the power generation side, a hybrid energy system, consisting of multiple main power supplies and ESSs, was considered. This work investigates an FC-battery hybrid SPS, however, the methodology is applicable to alternative generation and storage technologies as well. Furthermore, DC distribution offers several advantages, such as increased efficiency [24] and operational flexibility [5]. It is particularly suitable for DC sources, as is the case with FCs and batteries, which are interfaced via DCDC converters.

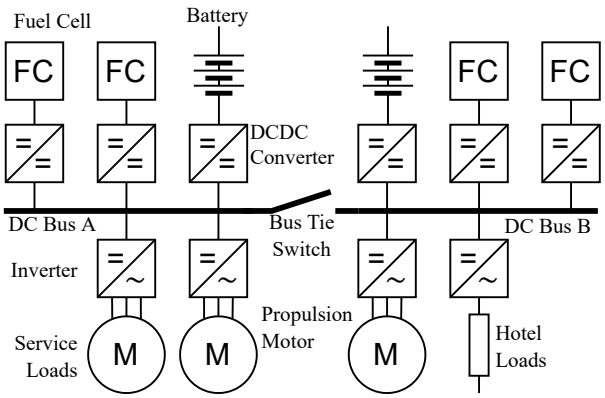

Figure 1: Power system topology of case study

A short-sea cargo vessel operating in the Baltic and North Sea, with a maximum propulsive power of $1.2\,\mathrm{MW}$, serves as a case study. The original system was fitted with a diesel direct-drive propulsion. For this research, a virtual retrofit of its SPS was conducted by fitting the vessel with an FC-battery hybrid system. The resulting system, equipped with four FC and two battery systems in a dual-bus configuration, is shown in Fig. 1. The power and energy ratings of the components are listed in Table 1. Real propulsive power measurements from various missions of the original system are available and used as inputs for the simulation of the SPS model. The comparably low hotel loads of the cargo vessel are neglected in the scope of this study.

Table 1: Case study parameters

Param.	Description	Value
V_{DC}	DC-link voltage	$700\,\mathrm{V}$
P_{FC}	FC power rating (x4)	$325\,\mathrm{kW}$
P_{bat}	Battery power rating (x2)	$325\,\mathrm{kW}$
C_{bat}	Battery capacity (x2)	$225\,\mathrm{kWh}$
P_{em}	Prop. motor rating (x2)	$600\,\mathrm{kW}$

The power rating of the batteries is selected such that one battery can deliver the same output power

as an FC at its peak, i.e., 325 kW. This allows short-time compensation for the loss of one main power supply via the batteries while still having a second battery covering transient loads.

3 MODELING

The focus of this work is the development of control strategies. Power system and component models are required to evaluate these strategies. Because the emphasis is on system-level control, simple dynamic models are implemented to build a simulation environment for the complete SPS. The following sections describe the approaches for modeling FCs, batteries and converters, and how they interact with one another and the load current via the DC-link.

3.1 Fuel Cell

The FC models used in this work were implemented according to [25]. A beneficial feature of this model is that it can be parameterized using manufacturer data. Hence, the real components can be easily represented.

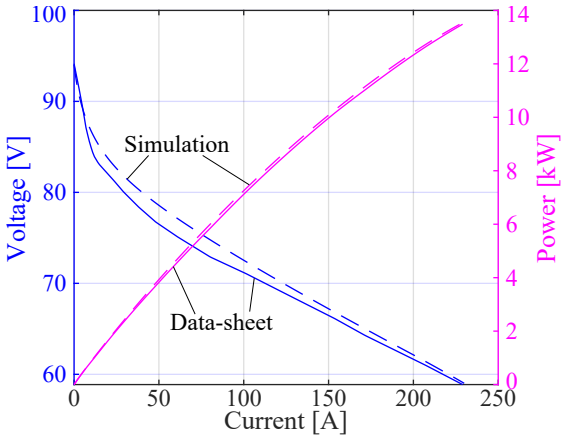

Figure 2: Polarization curve and power output of Nedstack FCS 13 XXL module, from data-sheet and simulation in steady-state

The FC systems investigated in this paper are based on the Nedstack FCS 13 XXL, a proton-exchange membrane fuel cell (PEMFC) module with a maximum output power of 13.6 kW [26]. To achieve the targeted 325 kW per FC system in the SPS, 24 modules are stacked together, with six parallel-connected strands of four modules in series. Figure 2 shows the polarization curves and power outputs of a single module from the manufacturer's data-sheet against the simulation results obtained using the described model in steady-state operation. The mean absolute percentage error (MAPE) of the output voltage between the simulation and data-sheet is 1.6 %, which is sufficiently accurate for the purpose of this research.

3.2 Battery

For the batteries, a model of similarly low fidelity as that for the FCs was used, as reported in [27]. It is based on single cell modeling, and in this study, generic values for Li-ion battery cells, as reported in the source, are used. Furthermore, multiple cells are connected in series and parallel such that the desired voltage, power, and energy levels of the battery packs are reached.

3.3 DCDC Converter

A dynamic model of a DCDC converter for maritime power systems is presented in [28]. It is an averaged model that describes the current dynamics while neglecting any losses in the system. Originally, the DCDC converter included a transformer stage. However, for the purpose of this paper, an averaged representation of a half-bridge is sufficient, and can be used as either a uni- or bi-directional converter, as in [29]. The dynamics of the average inductor current I_L in an ideal half-bridge topology can be computed as

$$\frac{dI_L}{dt} = \frac{1}{L}(V_{in} - (1-D)V_{out}) \qquad (1)$$

where V_{in} and V_{out} denote the source and output voltages, respectively; L is the main inductance and D the duty cycle of the switches, which functions as the control input. In the considered topology, the converter is directly interfaced to the DC bus, hence V_{out} equals the DC-link voltage V_{DC}. The DCDC converter is equipped with a PI current controller, tuned to operate at a bandwidth of 1 kHz. Hence, local controllers that generate the current reference for the DCDC converters can operate at 100 Hz.

3.4 DC-Link and Load

The DC distribution system in a ship is characterized by short lines with low impedance. For this reason, the DC-link can be modeled as a single capacitor, neglecting the losses and inductances in the network. The DC-link capacity C_{DC} is the sum of the output capacitors of all N adjacent DCDC converters $C_{out,i}$. Accordingly, the time derivative of the DC-link voltage $\dot{V}_{DC}$ can be computed as:

$$\dot{V}_{DC} = \frac{1}{C_{DC}}(\sum_{i=1}^{N} I_{out,i} - I_{load}) \qquad (2)$$

$$C_{DC} = \sum_{i=1}^{N} C_{out,i} \tag{3}$$

Furthermore, the load current can be derived from a given power profile P_{load} as

$$I_{load} = P_{load}/V_{DC} \tag{4}$$

4 COORDINATED CONTROL

The coordinated control in the FC-battery hybrid power system determines the current references for all integrated power generation and energy storage modules. This work focuses on the following three main functionalities of coordinated control in an SPS:

- (dynamic) Power sharing
- Voltage regulation
- SoC management

The importance of each of these three functionalities and a method for implementing them in a decentralized architecture are addressed in the following sections.

4.1 Dynamic Power Sharing

Virtual impedance-based droop control is used in this work to achieve the proposed modular characteristic for the coordinated control. The decentralized architecture of droop control schemes s fundamentally modular due to its lack of communication network. While traditional resistive droop control is appropriate for power sharing under steady-state conditions, additional capacitive or inductive droop elements can be used to improve power sharing under dynamic loads. The approach of using capacitive droop elements for DC microgrid control in [30] was applied to a HESS integrated into an SPS by [23] to achieve load frequency decoupling between different ESS technologies. Whereas a capacitive droop controller serves as a high-pass filter, this work proposes an extension of droop schemes with an inductive element to create a low-pass filter (LPF). Such a droop controller is an appropriate tool for controlling the power output of power supplies with slow dynamic capabilities, such as FCs. Figure 3 shows the equivalent circuits describing the functioning principle of different droop schemes. The corresponding transfer functions of the DC link voltage deviation $\Delta V = V_{ref} - V_{DC}$ to the current reference are as follows:

$$\frac{I_{d,R}}{\Delta V} = \frac{1}{R_{d,RL}} \tag{5}$$

$$\frac{I_{d,RC}}{\Delta V} = \frac{sC_{d,RC}}{sR_{d,RC}C_{d,RC} + 1} \tag{6}$$

$$\frac{I_{d,RL}}{\Delta V} = \frac{1}{R_{d,RL} + sL_{d,RL}} \tag{7}$$

where $I_{d,x}$ is the computed reference current for the droop-controlled source. $R_{d,x}$, $C_{d,x}$, and $L_{d,x}$ describe the virtual resistance, capacitance and inductance, C_{DC} isthe DC-link capacity; V_{ref} and V_{DC} are the reference and actual DC-link voltages, respectively.

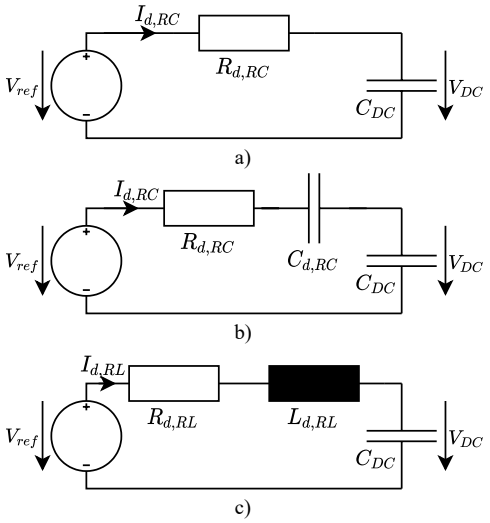

Figure 3: Virtual impedance control with a) classic resistive (subscript R) droop, b) resistive-capacitive (RC) droop, c) resistive-inductive (RL) droop

To achieve the desired frequency separation, a resistive-inductive droop scheme, as described by (7), is used in the local controllers of the FC systems. The battery controllers are equipped with a complementary resistive-capacitive droop controller according to (6). For the consistent behavior of the power system under dynamic operation, a series of guidelines for tuning the control parameters are proposed:

- The total droop resistance of the main power supplies and the ESS should be equal so that a consistent response of the power system in dynamic and steady-state operation is obtained.
- The total droop resistance should be selected such that the bandwidth of the DC bus voltage regulation is at least one order of magnitude slower than the current control of the DCDC converters.
- The droop resistances of the FC controllers should be inversely proportional to their rated power. The same approach shall be applied for the ESS.

- In the proposed FC-hybrid system, the time constants of the RC and RL filters should be equal, to allow a smooth transition from batteries to FC as a power source.
- Reducing the time constant will yield a higher dynamic capability, allowing the generation-side to cover higher load gradients, which would otherwise be inhibited by the limited power of the batteries. However, a higher time-constant lowers the output gradients of the FCs, reducing their degradation.

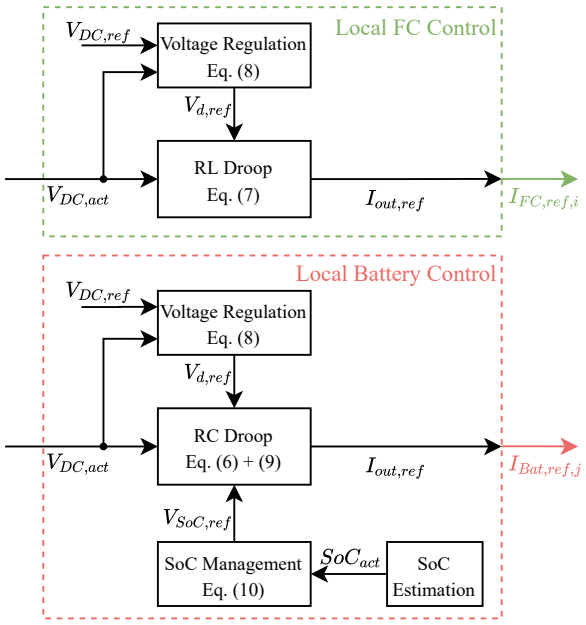

Figure 4: Decentralized control of FC and batteries with voltage regulation and SoC management

4.2 Voltage Regulation

It is desirable to maintain the DC link voltage at its nominal level to provide a certain quality of power supply and minimize transmission losses in the DC network. Traditional droop control schemes lead to a voltage drop on the main bus proportional to the delivered power [31]. For this reason, an additional voltage regulation function was added to the proposed droop-based power sharing strategy. A local implementation of this functionality maintains the modular control architecture. Hence, all the local controllers are equipped with an independent voltage regulation control. The proposed method is an integral adaptation of the reference voltage in the local droop controller based on the measured DC link voltage deviation. Accordingly, the voltage reference $V_{d,ref}$ in the local droop controllers of the sources is computed as:

$$V_{d,ref} = V_{DC,ref} + k_V \int V_{DC,ref} - V_{DC,act} dt \quad (8)$$

where k_V is the integral coefficient for voltage regulation and $V_{DC,ref}$ denotes the DC bus voltage reference. To avoid circulating currents between components, it is vital that deviations of $V_{d,ref}$ between local controllers are kept at a minimum. In the scope of this work, it is assumed that this can be achieved through an appropriate tuning of the control parameters. However, this challenge requires further attention in future research.

4.3 SoC Management

The limited energy capacity and power capability of battery storage systems act as constraints on the overall system control. The SoC management of ESS encompasses two main challenges.

First, it must be ensured that the SoC remains within certain boundaries, e.g. between 20 % and 80 % as in [32]. The usable energy is limited to account for capacity degradation, whereas deep discharge is avoided to prevent damagess and safety risks. Moreover, in steady-state the ESSs shall follow a reference SoC centered between the defined limits to withhold an equal positive and negative reserve for compensating load fluctuations.

Second, in the presence of multiple parallel ESS, differences in operation and parameter deviations lead to SoC imbalance. Hence, an additional objective of the power system control is to eliminate these imbalances under steady-state conditions.

These objectives imply the need for an extension of the control strategy by an SoC management functionality. As before, a decentralized approach is proposed. Because the SoC is an individual variable of every ESS, the coordination of this function between parallel devices is not required. An additional SoC-dependent term $V_{\mathrm{SoC},ref}$ is introduced to achieve the desired charge and discharge of the ESS. The adjusted reference voltage for the droop $V^*_{d,ref}$ is computed as:

$$V^*_{d,ref} = V_{d,ref} + V_{SoC,ref} \quad (9)$$

$$V_{\mathrm{SoC},ref} = k_{\mathrm{SoC}} \int (\mathrm{SoC}_{ref} - \mathrm{SoC}_{act})^{\alpha} dt \quad (10)$$

where SoC_{ref} and SoC_{act} are the reference and actual SoC values and k_{SoC} is the integral coefficient

of the SoC management strategy. The shape factor α describes the relationship between SoC deviation and charging current. Because the batteries use an RC droop controller, integration in (10) is required to produce the desired current.

Parameters k_{SoC} and α are selected such that the ESS provides its maximum discharge current $I_{ESS,max}$ at its maximum allowable charge. Accordingly, the minimum discharge current - $I_{ESS,max}$ is targeted at the lower SoC threshold to charge the ESS. Coefficient α determines the shape of the current reference over the SoC range. The curves for various values are plotted in Fig. 5. The smaller the value of $\alpha \in (0, \infty)$, the more stringently the SoC management function regulates the battery charge towards its reference value. A graphical representation of the local controllers for the FCs and ESSs is shown in Fig. 4.

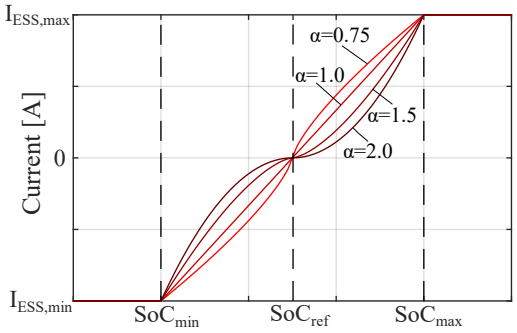

Figure 5: Relationship of individual battery SoC and targeted discharge current depending on shape factor α

5 SIMULATION RESULTS

The models of the SPS components as well as the methodology described in the previous section are implemented in MATLAB Simulink. Several simulation scenarios were constructed based on the case study described in Section 2 to evaluate and compare the proposed strategies to a benchmark controller.

5.1 Centralized Control with LPF

A centralized PI controller with an LPF was implemented as a benchmark, similar to the work in [21]. The central controller directly generates current references for all local controllers, requiring high-bandwidth communication. Furthermore, this strategy requires global awareness of all component parameters and states. The advantage of this architecture is that no coordination among the local controllers is required. It achieves accurate tracking of the reference DC link voltage as well as frequency decoupling according to the filter time constant τ_{LPF}.

The control strategy is illustrated in Fig. 6. The PI controller determines the reference current to stabilize and restore the DC link voltage. The low-frequency parts of this current are supplied by all FCs, while the batteries cover the remainder. The reference currents are distributed among parallel components proportional to their power rating.

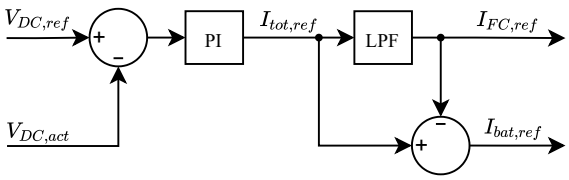

Figure 6: Centralized control strategy with LPF for frequency decoupling between FCs and batteries

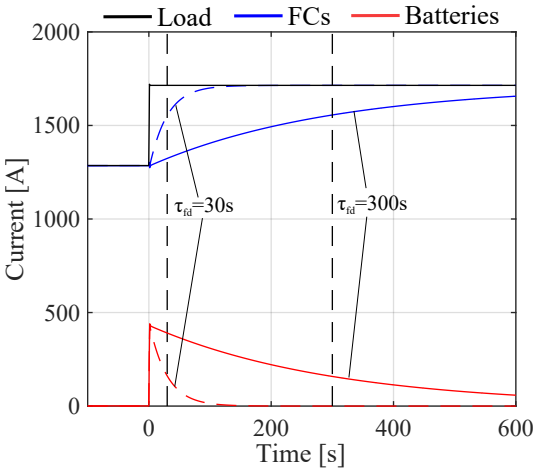

Figure 7: Total output current of FC and battery systems after a load step using the centralized PI control with LPF and time constants of 30s(dashed) and 300s(solid)

In the first simulation, the step response of the power system was investigated. Measurements of the propulsive power, taken during a mission of the reference cargo vessel, show an average load of 900 kW during cruising. Taking this value as the starting point, the step to full propulsive power of 1200 kW was investigated. In this scenario, the initial power load was assumed to be completely supplied by the FCs. To avoid high power gradients for the FCs, the LPF time constant τ_{LPF} was chosen to be in the range of multiple seconds to minutes. Two step responses with $\tau_{LPF} = 300\,\mathrm{s}$ and $30\,\mathrm{s}$ were analyzed to compare the effects of different time constants. The PI controller was tuned such that its poles are in the area of 10 Hz, approximately

10 times slower than the underlying current control.

The resulting step responses are displayed in Fig. 7. The FCs react to the load change according to the LPF; therefore at $t = \tau_{LPF}$ the output current reaches 63.2 % of its final value. The battery supplies the remaining difference between load and FC power, and additionally stabilizes the DC link voltage, which remains within 5 V of the nominal DC link voltage of 700 V.

5.2 Decentralized Control Strategy

The proposed strategy aims to achieve the same performance as the central controller using a decentralized architecture. For this purpose, the total droop resistance was chosen such that it equals the inverse of the proportional factor of the PI controller in the benchmark strategy. Furthermore, the time constant for frequency decoupling τ_{fd} is adjusted by sizing the virtual inductances and capacitances such that $\tau_{fd} = R_{d,rc}C_{d,rc} = L_{d,rl}/R_{d,rl}$.

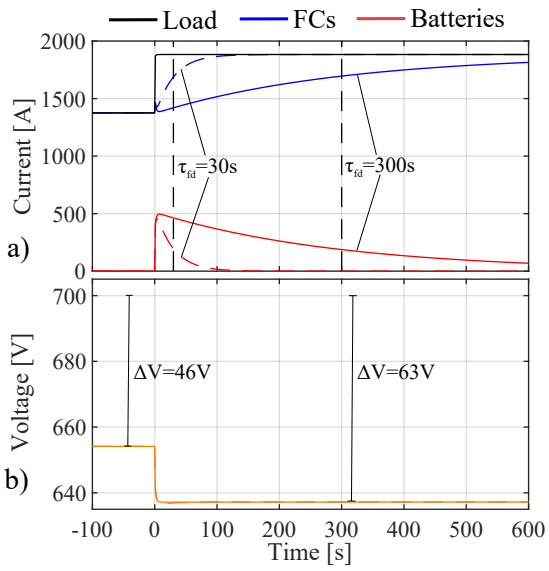

Figure 8: Load step response with decentralized strategy with τ_{fd}=30 s(dashed) and 300 s(solid) a) FC, battery and load currents, b) DC bus voltage

Initially, voltage regulation and SoC management are not implemented and the power system with the virtual impedance based droop is subjected to the same load step as the benchmark strategy in Section 5.1. The simulation results in Fig. 8 show that frequency decoupling is achieved as accurately as with the benchmark, matching the chosen τ_{fd}. The steady-state deviation resulting from the droop scheme, which lack an integral action, amounts to 63 V at full load. The reduced DC bus voltage requires higher currents and therefore increases conduction losses. Furthermore, the power quality can be insufficient for sensitive loads, and a sudden change in voltage is challenging for accurate current control in DCDC converters.

5.3 Voltage regulation

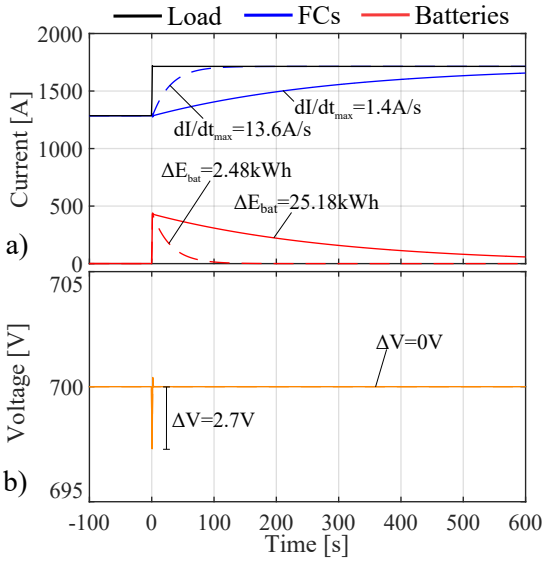

Figure 9: Load step response with decentralized strategy incl. voltage regulation with τ_{fd}=30 s(dashed) and 300 s(solid) a) FC, battery and load currents, b) DC bus voltage

In the next step, the same step response as before was simulated with the proposed strategy including the voltage regulation scheme described in Section 4.2. The gain k_V in (8) was selected to match the integral action of the benchmark's PI controller. Hence, the overall voltage control, tuned based on the DC bus capacitance, was designed to achieve a bandwidth of 100 Hz, ensuring that it is one order of magnitude slower than the local current control loops. It is vital to make k_V equal in all local controllers such that the same $V_{d,ref}$ is obtained. The differing dynamics and power ratings of the components are already represented in the virtual impedances. The step response obtained using this strategy is displayed in Fig. 9. The resulting curves of the FC and battery currents are equal to those of the benchmark, indicating that the same behavior of a centralized PI controller with an LPF can be achieved in a decentralized architecture. Additionally, this design of power sharing and voltage regulation achieves accurate tracking of the nominal DC bus voltage. Initially after the load step, a voltage drop of only 2.7 V can be observed with no steady-state error.

Furthermore, Fig. 9 shows the implications of changing the time constant τ_{fd}. With 300 s, a to-

tal of 25.18 kWh of battery charge is required to compensate for the difference between load and FC power, while the maximum current gradient of the FC systems is limited to 1.4 A/s. Reducing the time constant by a factor of ten, proportionally reduced the required battery charge. However, the current gradient of the FCs increased by the same factor, leading to higher degradation. This comparison highlights the underlying trade-off between the required battery charge and dynamic operation of the FCs when selecting the time constant.

5.4 SoC Management

To evaluate the SoC management function, described in Section 4.3, the SoCs of the two batteries were set to different initial values during the simulation. The constant load demand is entirely covered by the FCs, hence the batteries do not participate in load sharing and voltage regulation. The initial SoCs of batteries A and B are set to different values, as in [33]. Here, 70 % and 40 % were selected as the starting values. All batteries followed a reference SoC of 50 %. The shape factor α in (10) was set to 0.75, 1.0, 1.5 and 2.0, for a series of simulations.

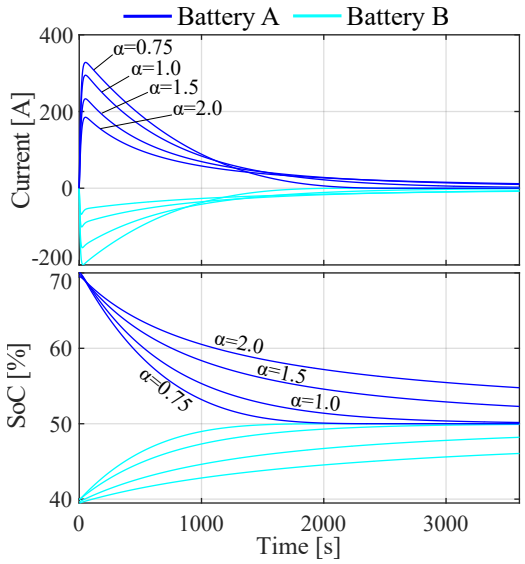

Figure 10: Convergence of two batteries' SoC towards reference value for different shape factors α

The resulting behaviors of the discharge current and SoCs over time for both batteries are shown in Fig. 10. As expected, a low shape factor yields a faster convergence towards the reference value. However, a high factor leads to a lower charging current, interfering less with other functionalities as long as the SoC is kept close to the reference. Additionally, the test case shows that different charges in parallel batteries are balanced over time.

5.5 Mission simulation

Finally, the complete proposed control strategy was evaluated using a realistic power profile from the reference short-sea cargo vessel. The considered mission, shown in Fig. 11, has a duration of ca. 30 h and was measured at 5 min intervals. For the simulation, running at 10 ms steps, the measured values were linearly interpolated.

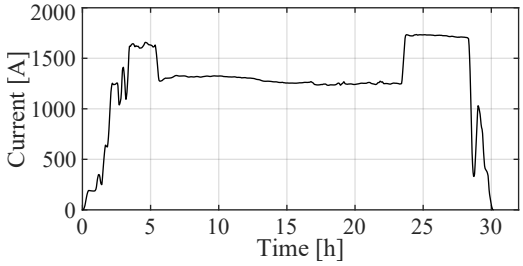

Figure 11: Power demand of exemplary mission used for the simulations

The focus of this investigation is to observe how the FCs' power output is adjusted when subjected to a real operating profile over a longer time and to what extent batteries are required to achieve a power balance. Three mission simulations were performed with varying time constants τ_{fd} for the frequency decoupling. Because multiple control functionalities act on the power system, it is key to ensure that they do not interfere with each other. As discussed in Section 5.3, the current and voltage control bandwidths are separated by tuning the control parameters. In the same manner, the slower control loops, i.e. the frequency decoupling and the SoC management, need to be separated to avoid them interfering with one another. For this purpose, the shape factor α was set to 2.0 so that the slope of the charging current around the target SoC was flat, reducing the charging dynamics as shown in Fig. 10. Doing so ensures that the SoC management acts more slowly than the frequency decoupling.

Figure 12 shows the resulting current curves of the FCs and batteries next to each other for the first segment of the mission profile until the vessel reaches a steady power demand at the cruising speed. Table 2 summarizes the key numbers from the simulations, including the batteries' SoC ranges, as well as maximum charge and discharge currents. Load cycling is reported to be detrimental to the health of PEMFC [34], [35]. In [36], a linear degradation factor for transient loads on the cell voltage decay was used. Hence, the average absolute value of the FC power gradient $|\dot{P_{FC}}|_{avg}$ is listed as a proxy for assessing the effect of FC operation on

degradation. Given the FC output $P_{FC,n}$ and time at the n-th simulation step t_n, it is computed as:

$$|\dot{P_{FC}}|_{avg} = \frac{1}{N}\sum_{n=1}^{N}\frac{|P_{FC,n} - P_{FC,n-1}|}{t_n - t_{n-1}} \quad (11)$$

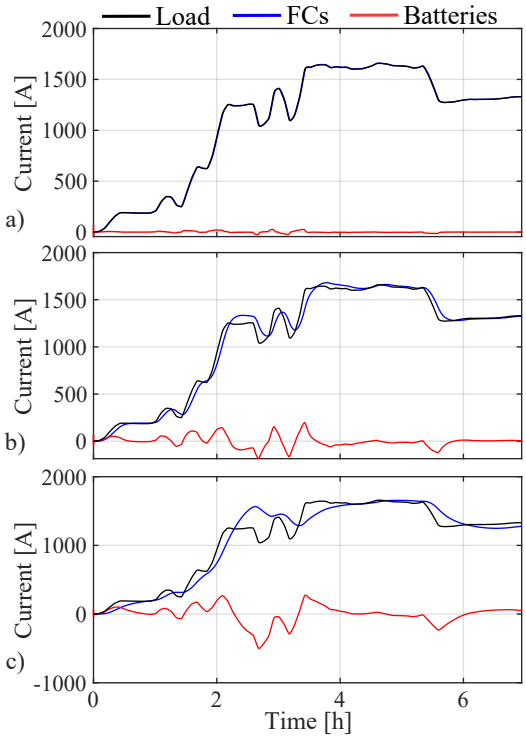

Figure 12: Total FC, battery and load currents with proposed strategy in mission simulation with τ_{fd}=30 s(a), 300 s(b) and 900 s(c)

Table 2: Evaluation of mission simulation

τ_{fd}	30 s	300 s	900 s
SoC_{min}	48.4 %	39.3 %	26.0 %
SoC_{max}	51.5 %	63.9 %	84.2 %
$P_{bat,min}$	−17 kW	−143 kW	−268 kW
$P_{bat,max}$	25 kW	121 kW	256 kW
$\|\dot{P_{FC}}\|_{avg}$	49.8 $\frac{W}{s}$	45.4 $\frac{W}{s}$	35.6 $\frac{W}{s}$

The results show that the FC follows the load closely, and little power and energy are demanded from the batteries with a low time constant. However, a higher time constant smoothens the power output of the FCs, reducing their power gradients and, consequently, their degradation. At a time constant of 900 s, the SoC-limits were fully exploited, leading to a minimized transient operation of the FCs. Overcharging above 80 % is caused by allowing a battery operation slightly above the batteries' ratings to avoid instability of the DC voltage. The results underscore the importance of selecting the time constant in a manner that aligns with the ship operator's objectives the trade-off between the discharge depth of the batteries and the transient loading of the FCs. It is important to note that an increased discharge depth negatively influences the battery lifetime, which must be considered in this trade-off. The simulated operation range of the batteries also shows that they may be sized significantly smaller when a small time constant is chosen to reduce capital expenditure.

6 CONCLUSIONS

Although FC-battery hybrid power systems with DC distribution are emerging as a promising solution for zero-emission shipping, the coordinated control of multiple power system resources remains a challenge. An appropriate control strategy can ensure power balance in the system while accounting for the different characteristics of the generation and storage technologies.

Especially in larger systems, a modular approach for integration and control appears to be a viable approach, as it can facilitate the reconfiguration and extension of the SPS by offering PnP capability. For this purpose, a decentralized coordinated control strategy based on virtual impedance droop controllers was presented as an alternative to centralized control. The proposed method achieves an excellent tracking of the DC bus voltage while decoupling the load power into low and high frequencies so that they can be covered by FCs and batteries, respectively. A trade-off is required between the dynamic operation of the main power supplies and the used power and energy of the batteries, affecting their degradation. This can be influenced by the time constant selection in the local droop controllers. It could be shown that the decentralized solution can achieve the same quality in dynamic power sharing and load tracking as a centralized PI controller with an LPF.

Hence, the developed method provides a decentralized control strategy capable of coordinating multiple power supplies and ESSs with different characteristics in large SPS. However, varying component parameters, e.g. owing to aging effects, and the effect of the operation strategy on system efficiency have not been accounted for in this study. Lack of awareness of specific system-wide parameters and variables in a decentralized architecture, e.g. the operating state and control parameters, are further challenges that will be addressed in future work. One possible solution is to investigate a low-

bandwidth communication network that can facilitate information sharing among local controllers. Furthermore. the introduction of a central controller enables the online adjustment of control parameters based on the operating conditions and changing component states and characteristics. The steady operation of FC already contributes to their efficient utilization. However, an explicit consideration and optimization of the overall system efficiency to reduce fuel consumption is planned.

ACKNOWLEDGMENTS

This research is supported by the *Sustainable Hydrogen Integrated Propulsion Drives (SH2IPDRIVE)* project, which has received funding from RvO (reference number MOB21013), through the RDM regulation of the Ministry of Economic Affairs and Climate Policy.

REFERENCES

[1] J. F. Hansen and F. Wendt, "History and State of the Art in Commercial Electric Ship Propulsion, Integrated Power Systems, and Future Trends," *Proceedings of the IEEE*, vol. 103, no. 12, pp. 2229–2242, Dec. 2015.

[2] M. U. Mutarraf, Y. Terriche, K. A. K. Niazi, J. C. Vasquez, and J. M. Guerrero, "Energy Storage Systems for Shipboard Microgrids—A Review," p. 32, 2018.

[3] C. Nuchturee, T. Li, and H. Xia, "Energy efficiency of integrated electric propulsion for ships – A review," *Renewable and Sustainable Energy Reviews*, vol. 134, p. 110 145, Dec. 2020.

[4] L. van Biert, M. Godjevac, K. Visser, and P. Aravind, "A review of fuel cell systems for maritime applications," *Journal of Power Sources*, vol. 327, pp. 345–364, Sep. 2016.

[5] L. Xu, J. Guerrero, A. Lashab, *et al.*, "A Review of DC Shipboard Microgrids—Part I: Power Architectures, Energy Storage, and Power Converters," *IEEE Transactions on Power Electronics*, vol. 37, no. 5, pp. 5155–5172, May 2022.

[6] M. S. Sadabadi, Q. Shafiee, and A. Karimi, "Plug-and-Play Robust Voltage Control of DC Microgrids," *IEEE Transactions on Smart Grid*, vol. 9, no. 6, pp. 6886–6896, Nov. 2018.

[7] H. Xing, C. Stuart, S. Spence, and H. Chen, "Fuel Cell Power Systems for Maritime Applications: Progress and Perspectives," *Sustainability*, vol. 13, no. 3, p. 1213, Jan. 2021.

[8] L. Xu, J. Guerrero, A. Lashab, *et al.*, "A Review of DC Shipboard Microgrids—Part II: Control Architectures, Stability Analysis, and Protection Schemes," *IEEE Transactions on Power Electronics*, vol. 37, no. 4, pp. 4105–4120, Apr. 2022.

[9] Y. Han, X. Ning, P. Yang, and L. Xu, "Review of Power Sharing, Voltage Restoration and Stabilization Techniques in Hierarchical Controlled DC Microgrids," *IEEE Access*, vol. 7, pp. 149 202–149 223, 2019.

[10] N. Shakeri, M. Zadeh, and J. Bremnes Nielsen, "Hydrogen Fuel Cells for Ship Electric Propulsion: Moving Toward Greener Ships," *IEEE Electrification Magazine*, vol. 8, no. 2, pp. 27–43, Jun. 2020.

[11] T. Dragicevic, X. Lu, J. Vasquez, and J. Guerrero, "DC Microgrids–Part I: A Review of Control Strategies and Stabilization Techniques," *IEEE Transactions on Power Electronics*, pp. 1–1, 2015.

[12] Z.-X. Xiao, Y.-Z. Guan, H.-W. Fang, Y. Terriche, and J. M. Guerrero, "Dynamic and Steady-State Power-Sharing Control of High-Efficiency DC Shipboard Microgrid Supplied by Diesel Generators," *IEEE Systems Journal*, vol. 16, no. 3, pp. 4595–4606, Sep. 2022.

[13] B. Zahedi and L. E. Norum, "Voltage regulation and power sharing control in ship LVDC power distribution systems," in *2013 15th European Conference on Power Electronics and Applications (EPE)*, Sep. 2013, pp. 1–8.

[14] C.-L. Su, X.-T. Weng, and Ching-Jin Chen, "Power generation controls of fuel cell/energy storage hybrid ship power systems," in *2014 IEEE Conference and Expo Transportation Electrification Asia-Pacific (ITEC Asia-Pacific)*, Beijing, China: IEEE, Aug. 2014, pp. 1–6.

[15] H. Chen, Z. Zhang, C. Guan, and H. Gao, "Optimization of sizing and frequency control in battery/supercapacitor hybrid energy storage system for fuel cell ship," *Energy*, vol. 197, p. 117 285, Apr. 2020.

[16] L. Balestra and I. Schjølberg, "Energy management strategies for a zero-emission hybrid domestic ferry," *International Journal of Hydrogen Energy*, vol. 46, no. 77, pp. 38 490–38 503, Nov. 2021.

[17] J. Han, J.-F. Charpentier, and T. Tang, "An energy management system of a fuel cell/battery hybrid boat," *Energies*, vol. 7, no. 5, pp. 2799–2820, 2014.

[18] A. M. Bassam, A. B. Phillips, S. R. Turnock, and P. A. Wilson, "Development of a multi-scheme energy management strategy for a hybrid fuel cell driven passenger ship," *International Journal of Hydrogen Energy*, vol. 42, no. 1, pp. 623–635, Jan. 2017.

[19] L. Zhu, J. Han, D. Peng, T. Wang, T. Tang, and J.-F. Charpentier, "Fuzzy logic based energy management strategy for a fuel cell/battery/ultracapacitor hybrid ship," in *2014 First International Conference on Green Energy ICGE 2014*, Mar. 2014, pp. 107–112.

[20] Z. Jin, L. Meng, J. C. Vasquez, and J. M. Guerrero, "Frequency-division power sharing and hierarchical control design for DC shipboard mi-

crogrids with hybrid energy storage systems," in *2017 IEEE Applied Power Electronics Conference and Exposition (APEC)*, Mar. 2017, pp. 3661–3668.

[21] K. Kwon, D. Park, and M. K. Zadeh, "Load Frequency-Based Power Management for Shipboard DC Hybrid Power Systems," in *2020 IEEE 29th International Symposium on Industrial Electronics (ISIE)*, Jun. 2020, pp. 142–147.

[22] P. Xie, S. Tan, N. Bazmohammadi, *et al.*, "A distributed real-time power management scheme for shipboard zonal multi-microgrid system," *Applied Energy*, vol. 317, p. 119 072, Jul. 2022.

[23] J. Khazaei, "Optimal Flow of MVDC Shipboard Microgrids With Hybrid Storage Enhanced With Capacitive and Resistive Droop Controllers," *IEEE Transactions on Power Systems*, vol. 36, no. 4, pp. 3728–3739, Jul. 2021.

[24] B. Zahedi, L. E. Norum, and K. B. Ludvigsen, "Optimized efficiency of all-electric ships by dc hybrid power systems," *Journal of Power Sources*, vol. 255, pp. 341–354, Jun. 2014.

[25] S. N. M., O. Tremblay, and L.-A. Dessaint, "A generic fuel cell model for the simulation of fuel cell vehicles," in *2009 IEEE Vehicle Power and Propulsion Conference*, Sep. 2009, pp. 1722–1729.

[26] *FCS 13-XXL — Nedstack*, https://nedstack.com/en/pem-fcs-stack-technology/fcs-13-xxl.

[27] O. Tremblay, L.-A. Dessaint, and A.-I. Dekkiche, "A Generic Battery Model for the Dynamic Simulation of Hybrid Electric Vehicles," in *2007 IEEE Vehicle Power and Propulsion Conference*, Sep. 2007, pp. 284–289.

[28] B. Zahedi and L. E. Norum, "Modeling and Simulation of All-Electric Ships With Low-Voltage DC Hybrid Power Systems," *IEEE Transactions on Power Electronics*, vol. 28, no. 10, pp. 4525–4537, Oct. 2013.

[29] A. Haseltalab, L. van Biert, H. Sapra, B. Mestemaker, and R. R. Negenborn, "Component sizing and energy management for SOFC-based ship power systems," *Energy Conversion and Management*, vol. 245, p. 114 625, Oct. 2021.

[30] X. Chen, J. Zhou, M. Shi, L. Yan, W. Zuo, and J. Wen, "A Novel Virtual Resistor and Capacitor Droop Control for HESS in Medium-Voltage DC System," *IEEE Transactions on Power Systems*, vol. 34, no. 4, pp. 2518–2527, Jul. 2019.

[31] S. Peyghami, H. Mokhtari, P. Davari, P. C. Loh, and F. Blaabjerg, "On Secondary Control Approaches for Voltage Regulation in DC Microgrids," *IEEE Transactions on Industry Applications*, vol. 53, no. 5, pp. 4855–4862, Sep. 2017.

[32] L. Balestra, "Design of Hybrid Fuel Cell/Battery Systems for Maritime Vessels," Doctoral Thesis, NTNU, 2022.

[33] M. U. Mutarraf, Y. Guan, Y. Terriche, *et al.*, "Adaptive Power Management of Hierarchical Controlled Hybrid Shipboard Microgrids," *IEEE Access*, vol. 10, pp. 21 397–21 411, 2022.

[34] E. Pahon, S. Jemei, N. Y. Steiner, and D. Hissel, "Effect of Load Cycling on the Performance of Fuel Cell Stacks," in *2019 IEEE Vehicle Power and Propulsion Conference (VPPC)*, Oct. 2019, pp. 1–4.

[35] M. Jourdan, H. Mounir, and A. El Marjani, "Compilation of factors affecting durability of Proton Exchange Membrane Fuel Cell (PEMFC)," in *2014 International Renewable and Sustainable Energy Conference (IRSEC)*, Oct. 2014, pp. 542–547.

[36] T. Fletcher, R. Thring, and M. Watkinson, "An Energy Management Strategy to concurrently optimise fuel consumption & PEM fuel cell lifetime in a hybrid vehicle," *International Journal of Hydrogen Energy*, vol. 41, no. 46, pp. 21 503–21 515, Dec. 2016.